RADIATIVE HEATING IN MSL ENTRY: COMPARISON OF FLIGHT HEATING DISCREPANCY TO GROUND TEST AND PREDICTIVE MODELS

Brett A. Cruden[(1)], Aaron M. Brandis[(1)], Todd R. White[(1)], Milad Mahzari[(1)], Deepak Bose[(2)]

[(1)]ERC Inc at NASA Ames, NASA Ames Research Center, MS 230-2, Moffett Field, CA 94035,
E-mail: Brett.A.Cruden@nasa.gov, Aaron.M.Brandis@nasa.gov, Todd.R.White@nasa.gov, Milad.Mahzari@nasa.gov
[(2)]NASA Ames Research Center, MS 230-2, Moffett Field, CA 94035,
E-mail: Deepak.Bose@nasa.gov

ABSTRACT

During the recent entry of the Mars Science Laboratory (MSL), the heat shield was equipped with thermocouple stacks to measure in-depth heating of the thermal protection system (TPS). When only convective heating was considered, the derived heat flux from gauges in the stagnation region was found to be underpredicted by as much as 17 W/cm^2, which is significant compared to the peak heating of 32 W/cm^2. In order to quantify the contribution of radiative heating phenomena to the discrepancy, ground tests and predictive simulations that replicated the MSL entry trajectory were performed. An analysis is carried through to assess the quality of the radiation model and the impact to stagnation line heating. The impact is shown to be significant, but does not fully explain the heating discrepancy.

1. INTRODUCTION

In 2012, NASA landed the Mars Science Laboratory (MSL), which included the Curiosity Rover, on the surface of Mars. The heat shield contained the MSL Entry, Descent and Landing Instrumentation (MEDLI) suite,[1] which measured, among other things, the in-depth temperature profiles at several locations on the heat shield. These measurements were made on the MEDLI Integrated Sensor Plugs (MISPs) that were located at 7 positions along the heatshield, and numbered according to their relative importance. Predictive models, accounting only for convective heating, were found to agree well with most of the heating profile until the peak of the heating pulse. The heating beyond the peak was underpredicted, by as much as 2x on the stagnation line (MISP1).

It has been previously suggested that mid-wave infrared (MWIR) radiation from hot CO_2 could cause noticeable heating during Martian entries[2]. Tests in the Electric Arc Shock Tube (EAST) facility measured MWIR radiative heating for conditions similar to the MSL trajectory and suggested the magnitude of this mechanism to be the same order as this discrepancy.[3] This paper presents the results of new experiments in the EAST facility which replicate the MSL entry trajectory and corresponding predictive calculations using the DPLR Computational Fluid Dynamics (CFD) code and NEQAIR radiation solver. The comparison of predictions against EAST data is made to assess the accuracy of the DPLR/NEQAIR results. Estimated radiative heating profiles are then obtained directly from EAST data, from the nominal DPLR/NEQAIR prediction and from DPLR/NEQAIR adjusted for experiment/model disagreements. These three profiles are then compared to the flight measurement and the impact is assessed.

2. EXPERIMENTAL APPROACH

The EAST facility has been described in some detail in previous publications.[4] Ideally, the shock tube flow represents a 1-D profile which has similarity to the stagnation line profile of a vehicle entering an atmosphere of identical composition, density and velocity. The MSL best estimated trajectory (BET) has been determined through analysis of the the Mars Entry Atmospheric Data System (MEADS)[5] and is shown in Fig. 1 in terms of velocity and pressure. Five points

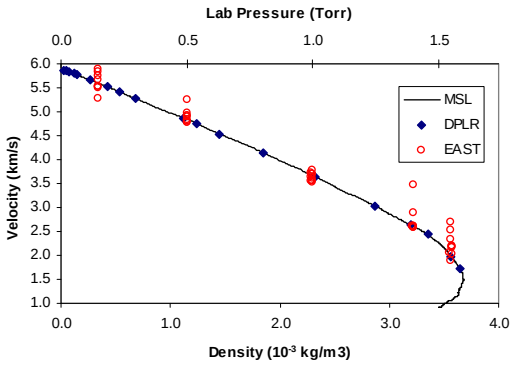

Figure 1. MSL Entry trajectory in terms of velocity/density. Test conditions in EAST and DPLR simulations are shown as points on the plot. Secondary x-axis indicates the pre-shock fill pressure corresponding to the required density.

on the MSL trajectory were chosen for testing in the EAST facility, and are summarized in Table I. A gas mixture consisting of 95.8% CO_2, 2.7% N_2 and 1.5% Ar (by volume) is used to approximate the Martian atmosphere. In testing, variability in velocity creates scatter around the nominal trajectory point that is apparent in Fig. 1. Points far from the trajectory are typically due to the iterative tuning procedure required to reach the desired condition and are not included in the analysis presented in this paper.

Table I. Selected entry conditions for shock tube testing

Time from Entry (s)	Density (g/m^3)	Velocity (m/s)	Pressure (Torr)
63.07	0.34	5600	0.15
73.80	1.15	4850	0.50
84.90	2.30	3610	1.00
96.00	3.21	2570	1.40
104.00	3.55	2050	1.55

Radiation from these shocks was measured from the Vacuum Ultraviolet (VUV) through Mid-Wave Infrared (MWIR) using instrumentation described previously.[6, 7] The instrumentation ranges are given in Table 2. While the objective was to obtain as much spectral signature as possible, ranges are limited by the lowest resolution grating available for each spectrometer. For this trajectory, the most important spectral ranges are identified as those corresponding to fundamental (4.3 μm) and overtone (2.7 μm) stretches of CO_2. These data sets must be collected in two separate shots as only one MWIR camera is in operation. The other spectrometers are set to cover a visible/near infrared (Vis/NIR: 480-900 nm), ultraviolet (UV/Vis: 200-500 nm over two shots) and vacuum ultraviolet (120-210 nm over two shots) ranges. Below 4 km/s, any signal in the vacuum ultraviolet is below the noise threshold of the camera, so the collection range is truncated at 145 nm. For each trajectory point and wavelength range, 2-3 shots were taken within 0.15 km/s of the target velocity. For most of the conditions here, the cameras were operated with a 2 μs exposure time, over which the shock may move by 4-10 mm, depending on velocity.

Table II. Wavelength ranges of the 4 spectrometers

Spectrometer	Range #1	Range #2
VUV	164-218	117-173
UV/Vis	323-497	190-352
Vis/NIR	472-890	
MWIR	3959-5403	1966-3405

3. COMPUTATIONAL APPROACH

Flowfield calculations are performed with the DPLR v4.02.2 non-equilibrium Navier-Stokes CFD solver.[8] The solutions are performed along the BET incorporating MEADS and Inertial Measurement Unit flight data.[5] The flow around the heatshield is modelled as thermochemical non-equilibrium flow using the Mitcheltree and Gnoffo 8-species (CO_2, CO, N_2, O_2, NO, C, N, and O) 12-reaction Mars model.[9] The Martian atmosphere is modeled as 97% CO_2 and 3% N_2 by mass. TPS surfaces are treated as a non-porous, non-slip, radiative equilibrium wall with constant emissivity (ε = 0.89) and the Mitcheltree/Gnoffo surface catalycity model. These assumptions are the same as those used for heating reconstruction[1], but differ from the design which used the conservative, but non-physical, super catalytic assumption.[10]

Lines of sight were extracted from the DPLR solutions at locations corresponding to the stagnation line, where the MISP 1 plug is located. NEQAIR simulations were conducted to obtain the spectral radiance along the stagnation line and the equivalent radiative heating under the tangent slab approximation. NEQAIR v14.0, which contains a CO_2 molecular line list based on the carbon dioxide spectal databank (CDSD-4000) was used.[11, 12] This update was critical to obtaining realistic simulations of the radiative heating for the MSL entry environment. The NEQAIR simulations of the radiative heat flux for MEDLI are integrated from 85.5 nm to 20000 nm.

4. EXPERIMENTAL RESULTS

Representative EAST Experiments are shown in Fig. 2. The figures show 3D measurements with wavelength on the x-axis and position on the y-axis. The shock is located at approximately 2 cm on the axis. Figure 2(a,b) represent the early entry time of t = 63s. In this portion of the trajectory, measurable levels of radiation are observed in both the ultraviolet (Fig 2a) and mid-infrared (Fig 2b). Non-equilibrium is observed with the overshoot at the shock front which then relaxes toward an equilibrium level of radiation behind the shock. Evidence of the end of the test is apparent in Fig. 2a where the radiance increases due to contamination at 9 cm. The spectral signature in the ultraviolet is comprised of electronic transitions of CO and NO while the MWIR is from vibrational transitions of CO and CO_2. While the magnitude in spectral radiance is similar for the two plots, the MWIR band spans a significantly larger wavelength range so will contribute more significantly to the integrated spectral radiance, and hence heat flux.

Later in the trajectory, (Fig. 2c,d) features in the ultraviolet through visible become negligible and the

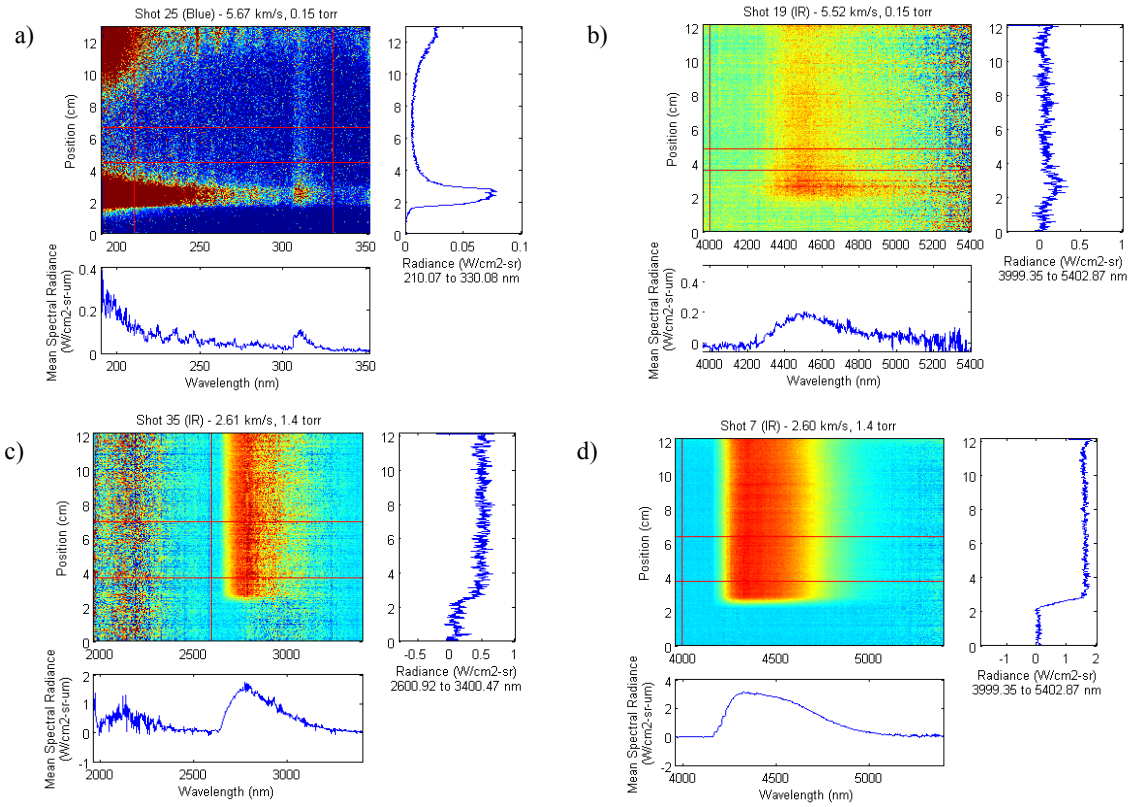

Figure 2. Measurement of radiance versus wavelength and position for representative shock conditions. (a,b) t=63 s, 5.6 km/s (nominal), 0.15 Torr and (c,d) t = 96 s, 2.6 km/s, 1.4 Torr.

MWIR bands strengthen. Two bands are observed at intensities that are an order of magnitude higher than at t=63 s. The shock shape is nearly a step function with no obvious non-equilibrium overshoot or relaxation. This is due to the higher density allowing for greater collisions and fast equilibration. For the shock tube diameter of 10 cm, evidence of blackbody saturation is apparent for the 4.3 μm band as its peak is flattened. For these two cases, no evidence of contamination or contact front arrival is observed. It should be noted that the sensitivity of the optics and spectrometer are lowered from 2-2.3 μm, such that the noise in this region obscures any real signal. A reduced sensitivity is also apparent in the noise around 3 μm, though in Fig 2c the signal is sufficiently strong to rise above this.

The summary of measurements at all five conditions is shown in Figure 3. Here the cross-section of spectral radiance from 2-4 cm behind the shock front is averaged and presented for the UV-Visible and Mid-Infrared regions. Due to differences in noise floors

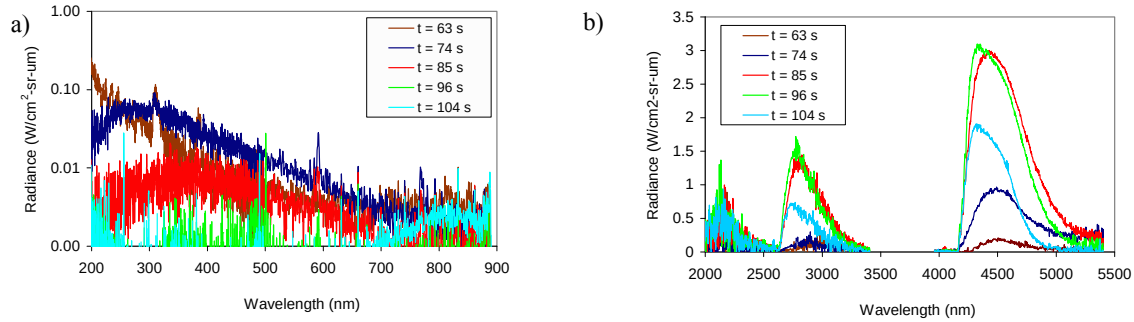

Figure 3. Radiance behind the shock at 5 trajectory points. (a) UV-NIR wavelengths, (b) MWIR wavelength.

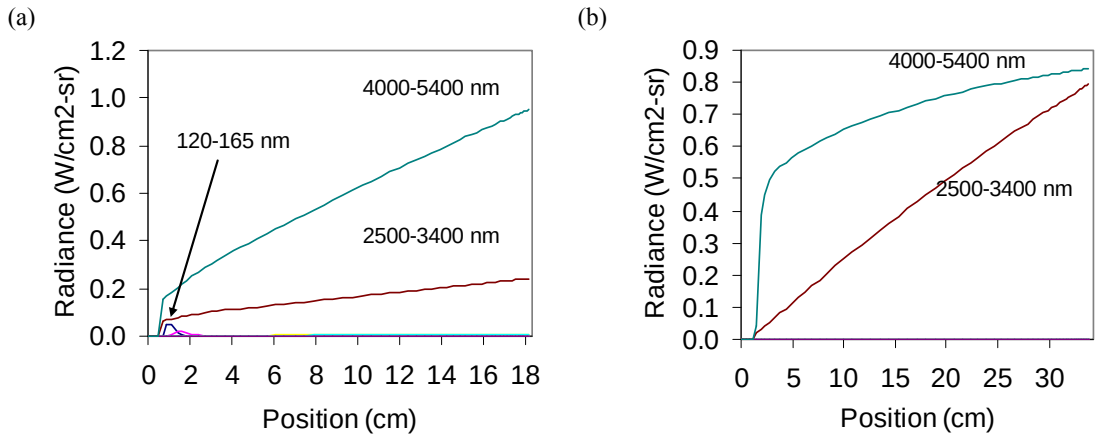

Figure 4. Radiance accumulated over position from EAST data analysis. (a) t=74 s, (b) t=104 s.

between different cameras, the VUV data is not shown and the MWIR data is presented in a separate plot from the UV-NIR data. In the UV-NIR range, the radiance is seen to decrease throughout the trajectory. At the same time the location of maximum radiance moves to higher wavelengths due to the blackbody limit changing as temperature is reduced. At t = 96 s and beyond, the signal is no longer distinguished from the noise level of the camera. In the mid-infrared, on the other hand, radiance is increasing through the trajectory until t = 85-96 s where the signal reaches its maximum level before decreasing at t = 104s. This increase is attributed to a rising CO_2 density as the shock density increases and its dissociation rate decreases. Near the end of the trajectory, the lower temperature causes the radiance to begin decreasing again. The level of the MWIR radiance is orders of magnitude larger than in the visible range (note that a log scale is used in Figure 3a). Furthermore, the features span a wavelength range that is several times larger than the visible wavelengths, so will dominate the radiative heating.

In order to compare the shock tube measurements to the flight heating data, it is necessary to adjust for geometric factors. A procedure for doing this has been presented in [13], and is summarized here. On the vehicle, the radiative heating will be collected along lines of sight originating outward from the detector location on the heat shield. Under the similarity assumption, the EAST facility measurements characterize the radiance perpendicular to the vehicle's stagnation line. This radiance versus position is converted to a volumetric emission coefficient using an assumed temperature profile. The emission coefficient and temperature profile are then used with the radiative transport and tangent slab approximation to obtain an equivalent stagnation point heat flux.

To perform this computation, two different temperature profiles have been assumed. The first uses the best practices profile of DPLR using the Mitcheltree chemistry.[9] Heating is integrated from the shock front to the boundary layer edge. (Predicted boundary layer aborption is <3% so is neglected). The second approach uses the EAST data itself by calculating the blackbody temperature that bounds the data. The temperature profile obtained this way is extrapolated using a best-fit exponential decay toward equilibrium. The integration is carried through the shock stand-off distance derived by CFD. The intent of exploring this method of temperature determination is to separate model dependencies from a purely experimental determination of heat flux, although the result is still dependent upon the shock standoff distance derived by CFD.

The integration of radiance along the stagnation line of sight is shown in Figure 4 as a function of position from the edge of the CFD domain. At the low pressure condition (Figure 4(a)), the non-equilibrium contribution from the VUV is initially apparent but then decreases as it is reabsorbed in the body of the shock layer. Radiation from the 2.7 and 4.3 μm bands increases linearly with position, as would be expected for an optically thin radiator. Later in the trajectory (Figure 4 (b)), the 4.3 μm band is seen to quickly rise and then slowly increase beyond the shock front. The plateau is attributed to the optical thickness of the band. The radiance increases slowly at longer distance as radiance from the outer edges of the band accumulates to their blackbody limits. The 2.7 μm band, on the other hand, increases linearly, indicating it remains optically thin over 35 cm.

The heat flux obtained from these approaches is shown in Figure 5. The error bars represent the variation (standard deviation) between tests at similar

conditions, weighted by the relative contribution of the different wavelength ranges. The x-error bars indicate the range of velocities analyzed and where they correspond to in MSL entry time. The DPLR solutions are obtained at slightly different conditions than those in Table I but are always contained within the x-error bar range (see Figure 1).

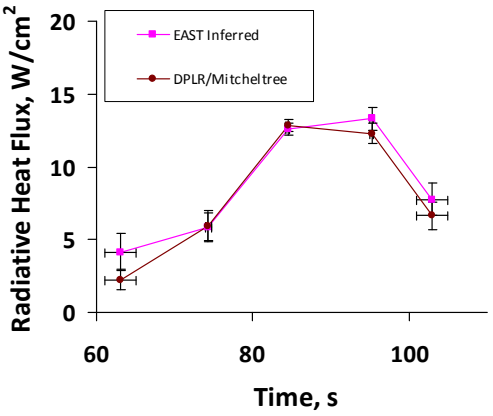

Figure 5. Radiative heat flux inferred from EAST experiments. The different curves represent the heat fluxes obtained assuming temperature profiles obtained through different methods.

5. VALIDATION OF NEQAIR SIMULATIONS AGAINST EAST EXPERIMENTS

Figure 6 shows a comparison of the radiance versus position from the 4.3 μm band in the EAST data and for the DPLR/NEQAIR stagnation line simulation corresponding to the MSL entry time of 84 s (velocity of approximately 3.7 km/s). Excellent agreement is obtained, and it is clear from this plot that neither CFD nor experiment have sufficient time to relax to equilibrium. Therefore, an assessment of the equilibrium radiation prediction is not generally possible for these tests.

Due to limitations in test time and the physical window length, the EAST experiment cannot replicate the radiance over the entire shock stand-off distance. Therefore, in order to assess the level of agreement between EAST and the simulation results, the temporal traces are integrated ±2 cm from the shock front location. This integrated value is here referred to as the "Absolute Nonequilibrium Radiance," as discussed in our previous publications.[13, 14] This comparison is used to provide a bounding factor for the accuracy of the simulation, which is otherwise completely independent of the EAST data. This comparison is shown for the two dominant spectral regions in Figure 7(a). Near peak radiative heating, these two spectral regions comprise approximately 90% of the total radiative heat flux. Though the data is displayed as a function of velocity, the pressure is also changing throughout the test points as represented by Figure 1. As suggested by Figure 6, generally good agreement is obtained over the 3959 to 5000 nm range. A slight shift in velocity space is apparent - increasing the experimentally measured velocity by 0.2 km/s would result in a near perfect agreement. The velocity accuracy, however, is believed to be better than 0.05 km/s. While in previous publications we have postulated that the affect of shock deceleration may appear similar to an increased velocity,[15, 16] this is not expected to be noticeable within 2 cm of the shock front. The alternative would be to attribute the difference to the kinetic model, as we have explored in previous publications.[7] As shown in that work, different models match the data at different velocities, the result of which would be a shift when the data is compared to only one model as a function of velocity.

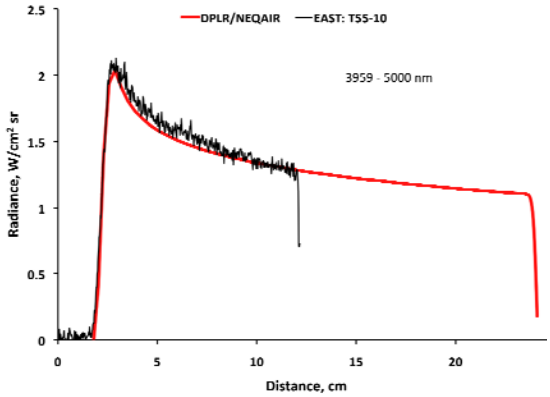

Figure 6. Spatial comparison of DPLR/NEQAIR with EAST.

The simulations under-predict the 2600 to 3404 nm range by as much as a factor of three, as was shown in our previous publication for similar conditions.[7] It has been suggested that the spectroscopic constants for this band may require refinement.

Regardless of the reason for mismatch to experiment, the radiative heating prediction can be assigned an uncertainty that is carried through to the margin determination for heat shield sizing purposes. Here, we quantify the uncertainty by the level of disagreement of the prediction to shock tube data. This is expressed as a ratio in Figure 7(b) for both the 2.7 and 4.3 μm band, which displays the disagreement for discrete points and best fit lines through the ratio. A further band can be placed upon the ratio to encompass all data points, as shown by the dotted lines. Though the 2.7 μm band is significantly underpredicted, it is

generally less important in terms of the overall radiative heating, being between 15-25% as strong as the 4.3 μm band. The overall uncertainty factor is then weighted by the relative contribution of each band to the total heat flux. The NEQAIR/DPLR prediction can then be scaled by this factor to obtain a "corrected" NEQAIR heat flux, as discussed in the next section.

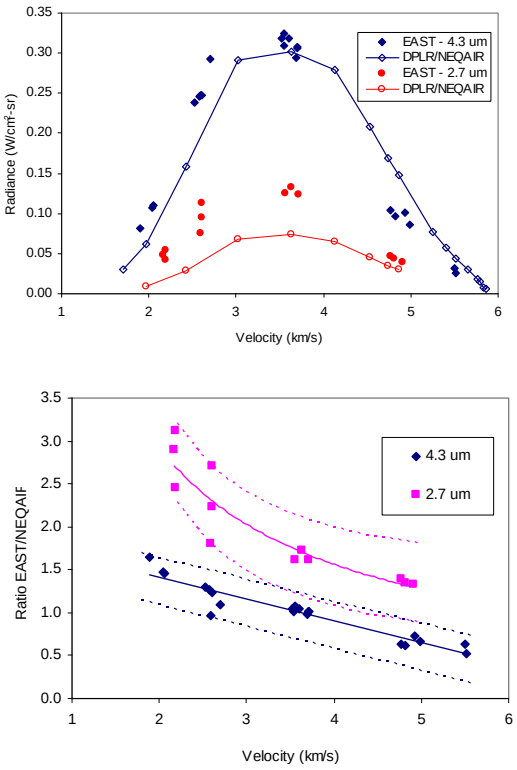

Figure 7. (a) Comparison of DPLR/NEQAIR simulations with EAST for dominant spectral ranges of 2600-3404 nm and 3959-5000 nm. (b) Margin factors for scaling radiative data to experiment. The solid line displays the nominal scaling factor while the dotted lines give the band of scaling factors to encompass all data points.

6. PREDICTED RADIATIVE HEAT FLUX

Figure 8 shows the radiative heating as predicted by DPLR and NEQAIR for MISP1. The radiative heating peaks at approximately 12 W/cm^2, and later in the trajectory when compared to peak convective heating. Also shown is the corrected NEQAIR heat flux and the experimentally derived heat flux discussed in Section 4. The experimentally derived heat flux is greater than the NEQAIR prediction at all times but displays the same peak location at approximately 14 W/cm^2. The corrected NEQAIR data is lower than the experimentally derived flux during the rising pulse and is higher at the peak and later times. The difference in the rising pulse is attributed mostly to noise in the measurement of the 2.7 μm band, leading to an overestimate of radiative heat flux in the EAST inferred heat flux. The difference at peak and cool down comes from using the correction factor derived within 2 cm of the shock front across the entire shock thickness, which may make the corrected heat flux overly conservative. The error bars on the corrected heat flux originate from the bounding bands given in Figure 7(b) and are as large as 4 W/cm^2 at peak heating. This error is conservative, however, as it is driven more by the disagreements at low velocity than at the peak condition.

Comparison of the radiative heating to the flight data unfortunately is not straightforward. The flight data is analyzed through an inverse analysis approach.[17] The inverse analysis essentially iterates backward through the material response code to obtain a surface heating profile that matches in-depth thermocouple measurements. The heating profile obtained is unable to separate heating terms attributable to environmental factors (i.e. convective and radiative heating) from thermal transport driven by material decomposition and blowing. The inverse analysis also requires a recession profile as input. The recession profile is obtained by running the nominal environmental heating as input. Therefore, any changes to the nominal environment require re-evaluation of the inverse analysis with a new recession profile. Confidence intervals are obtained from a Monte Carlo analysis,[17] including a constant recession scaling, but does not account for epistemic (i.e. model) uncertainties.

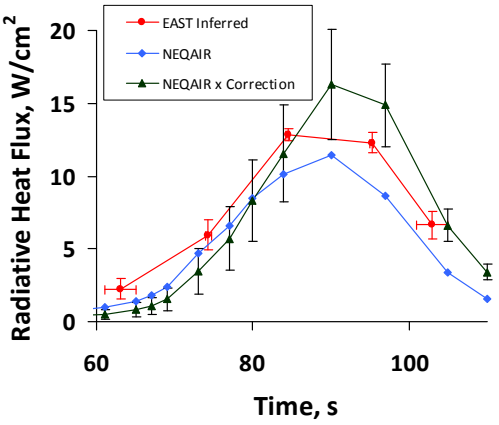

Figure 8. Radiative heating for MISP1 derived from experiment, prediction and prediction+experimental correction factor.

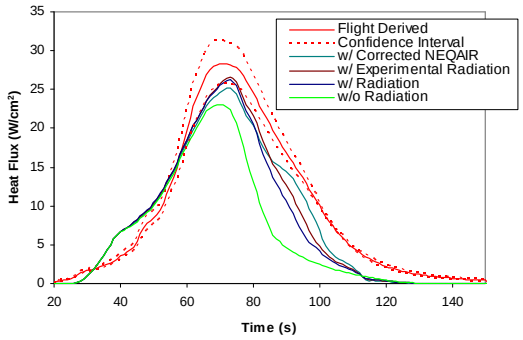

Figure 9. Comparison of heat flux profiles obtained with the three radiation analyses and with convection only. Flight data from inverse analysis is also shown with its confidence interval

The three profiles from Figure 8 are then processed through the FIAT material response code, along with convective heating terms (film coefficient, recovery enthalpy) to obtain a heating profile which can be compared to the inverse analyzed flight data. The profiles of Figure 8 are not simply additive to the convective heating as the heat shield responds by rejecting between 30-50% of the additional heat flux by thermal radiation, reflection/scattering, and ablation/blowing. The curves shown in Figure 9 represent the heat flux corrected by FIAT's prediction of the latter two effects, in order to be compared to the inverse analysis. The surface thermal radiation is calculated and accounted for in both the forward and inverse FIAT heat balances, so is not included in Figure 9.

The inclusion of radiation is here seen to increase the peak heat flux to nearly coincide with the lower limit of the confidence interval. Additionally, the peak location has shifted in time to agree with the flight data. At later times in flight, however, the heat flux remains underpredicted by more than the confidence interval allows. The amount of underprediction is approximately halved versus convection alone. Reasons for the underprediction at late times are not presently understood, though it is speculated that the wall enthalpy may be incorrectly predicted based on the equilibrium recession/ablation model used by FIAT. The three different radiation curves are qualitatively similar, though the corrected NEQAIR profile shows an inflection which is not apparent in the other data sets. This is believed to be due to an overly conservative correction factor at late times rather than an improved prediction of heat flux.

The impact in terms of heat load is shown in Fig. 10. Heat load, as the integral of heat flux, is a more relevant quantity in terms of heat shield sizing. The heat load shown has been corrected for ablation/blowing as necessitated by the inverse analysis. The median heat load estimated from the flight sensors is 1200 J/cm^2 with a 95% confidence interval of ± 100 J/cm^2. The heat load found from convection alone underpredicted this heat load by 400 J/cm^2, or 33%. Including radiation with the nominal NEQAIR/DPLR prediction reduces the error to 230 J/cm^2, or 19%. Also shown are the heat loads obtained using the experimentally derived and corrected NEQAIR heating. These display errors of 16% and 14%, respectively. This error is still greater than the confidence interval, so would need to be carried as a margin factor in future sizing exercises.

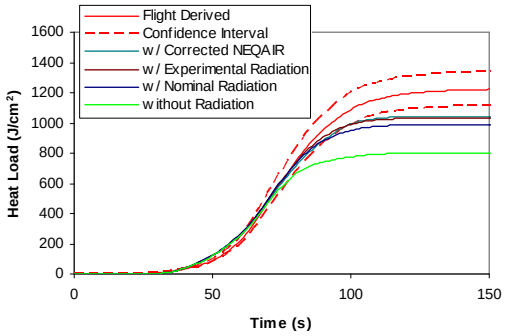

Figure 10. Heat Load determined from flight data and predicted with and without radiation terms.

7. CONCLUSIONS

The underprediction of flight heating profile in the recent MSL entry is investigated in terms of radiative heating contribution, which was not included in the original analysis. This work considers the possibility that vibrationally hot CO_2 may contribute sufficient emission to impact the heat flux and heat load during entry. To do this, the radiative heating is simulated using the NEQAIR code based on flowfields calculated with DPLR and is measured in the Electric Arc Shock Tube facility. Radiation in the VUV through Near Infrared are shown to be negligible in comparison to the mid-infrared radiation. The two major bands of CO_2 (4.3 μm and 2.7 μm) are characterized.

Comparing the NEQAIR simulations to the EAST data indicate the 4.3 μm band to be matched to within a velocity shift of 0.2 km/s. This disagreement is suggested to be related to the kinetic model used in the CFD solution. The 2.7 μm band is underpredicted by as much as 3x, with the error decreasing at higher velocity. This error is mostly attributed to the spectral database.

The radiative heat flux expected based on the MSL trajectory is then generated in three different ways. First, NEQAIR is used to directly simulate the radiative heating magnitude. Second, geometric arguments are used to infer a radiative heating directly from the EAST data, although this magnitude is still dependent upon the DPLR temperature profile. Finally, a correction factor for NEQAIR is determined based on EAST simulations and applied across the flight profile. These three methods yield a peak radiative heat flux of 12, 14 and 16 W/cm^2, respectively, and peak later in time than the convective pulse.

The heat flux based on NEQAIR has been used with the material response code to determine a heating that may be compared to that obtained via inverse analysis of the flight data, and is shown to improve predictions. The error in heat load is reduced from 33% to 19% by inclusion of radiation. This error is still outside of the confidence intervals of the flight data, suggesting further model deficiencies exist. It is speculated that using a finite rate ablation chemistry model will improve the agreement.

8. ACKNOWLEDGEMENTS

The authors would like to thank NASA's Entry Systems Modeling (ESM) project and MEDLI for their support of this work. Drs. Cruden, Brandis, Mahzari and White are supported through the NNA10DE12C contract between NASA Ames Research Center and ERC Inc.

9. REFERENCES

1. Bose, D., White, T., Mahzari, M., and Edquist, K., "Reconstruction of Aerothermal Environment and Heat Shield Response of Mars Science Laboratory," Journal of Spacecraft and Rockets, Vol. 51, No. 4, 2014, pp. 1174-1184.
2. da Silva, M. L., and Beck, J., "Contribution of CO2 IR Radiation to Martian Entries Radiative Wall Fluxes," 49th AIAA Aerospace Sciences Meeting. AIAA, Orlando, FL, 2011, AIAA 2011-135.
3. Cruden, B. A., Prabhu, D., and Martinez, R., "Absolute Radiation Measurement in Venus and Mars Entry Conditions," Journal of Spacecraft and Rockets, Vol. 49, No. 6, 2012, pp. 1069-1079.
4. Cruden , B. A., "Absolute Radiation Measurements in Earth and Mars Entry Conditions ", Technical Report RTO-EN-AVT-218, NATO.
5. Karlgaard, C., Kutty, P., Shidner, J., Schoenenberger, M., and Munk, M., "Mars Entry Atmospheric Data System Trajectory Reconstruction Algorithms and Flight Results," AIAA 2013-0028.
6. Cruden, B. A., Martinez, R., Grinstead, J. H., and Olejniczak, J., "Simultaneous Vacuum Ultraviolet through Near IR Absolute Radiation Measurement with Spatiotemporal Resolution in an Electric Arc Shock Tube," 41st AIAA Thermophysics Conference. AIAA, San Antonio, TX, 2009, AIAA 2009-4240.
7. Cruden , B. A., Prabhu, D. K., and Brandis, A. M., "Measurement and Characterization of Mid-wave Infrared Radiation in CO2 Shocks," AIAA Paper 2014-2962.
8. Wright, M. J., Candler, G., and Bose, D., "Data-Parallel Line Relaxation method for the Navier-Stokes Equations," AIAA Journal, Vol. 36, No. 9, 1998, pp. 1603-1609.
9. Mitcheltree, R. A., and Gnoffo, P. A., "Wake Flow About a MESUR Mars Entry Vehicle," AIAA-94-1958.
10. Edquist, K., Dyakonov, A., Wright, M., and Tang, C., "Aerothermodynamic Design of the Mars Science Laboratory Heatshield," AIAA 2009-4075.
11. Palmer, G., and Cruden, B., "Experimental Validation of CO2 Radiation Simulations," AIAA Paper 2012-3188.
12. Tashkun, S. A., and Perevalov, V. I., "CDSD-4000: High-resolution, high-temperature carbon dioxide spectroscopic databank," Journal of Quantitative Spectroscopy and Radiative Transfer, Vol. 112, 2011, pp. 1403-1410.
13. Cruden, B. A., "Radiance Measurement for Low Density Mars Entry," AIAA Paper 2012-2742.
14. Brandis, A. M., Johnston, C. O., Cruden, B. A., and Prabhu, D. K., "Investigation of Nonequilibrium Radiation for Mars Entry," AIAA Paper 2013-1055.
15. Brandis, A. M., Cruden, B. A., Prabhu, D., Bose, D., McGilvray, M., and Morgan, R. G., "Analysis of Air Radiation Measurements Obtained in the EAST and X2 Shocktube Facilities," 10th AIAA/ASME Joint Thermophysics and Heat Transfer Conference. Chicago, IL, 2010.
16. Cruden, B. A., Brandis, A. M., and Prabhu, D. K., "Compositional Dependence of Radiance in CO2/N2/Ar Systems," AIAA 2013-2502.
17. Mahzari, M., White, T. R., Braun, R., and Bose, D., "Inverse Estimation of the Mars Science Laboratory Entry Aerothermal Environment and Thermal Protection System Response," AIAA 2013-2780.